JACS
JOURNAL OF THE AMERICAN CHEMICAL SOCIETY

Communication

pubs.acs.org/JACS

Total Structure Determination of $Au_{21}(S\text{-}Adm)_{15}$ and Geometrical/Electronic Structure Evolution of Thiolated Gold Nanoclusters

Shuang Chen,[†,∥] Lin Xiong,[‡,∥] Shuxin Wang,[*,†] Zhongyun Ma,[‡] Shan Jin,[†] Hongting Sheng,[†] Yong Pei,[*,‡] and Manzhou Zhu[*,†]

[†]Department of Chemistry and Center for Atomic Engineering of Advanced Materials, Anhui University, Hefei, Anhui 230601, People's Republic of China

[‡]Department of Chemistry, Key Laboratory of Environmentally Friendly Chemistry and Applications of Ministry of Education, Xiangtan University, Xiangtan, Hunan 411105, People's Republic of China

Supporting Information

ABSTRACT: The larger size gold nanoparticles typically adopt a face-centered cubic (fcc) atomic packing, while in the ultrasmall nanoclusters the packing styles of Au atoms are diverse, including fcc, hexagonal close packing (hcp), and body-centered cubic (bcc), depending on the ligand protection. The possible conversion between these packing structures is largely unknown. Herein, we report the growth of a new $Au_{21}(S\text{-}Adm)_{15}$ nanocluster (S-Adm = adamantanethiolate) from $Au_{18}(SR)_{14}$ (SR = cyclohexylthiol), with the total structure determined by X-ray crystallography. It is discovered that the hcp Au_9-core in $Au_{18}(SR)_{14}$ is transformed to a fcc Au_{10}-core in $Au_{21}(S\text{-}Adm)_{15}$. Combining with density functional theory (DFT) calculations, we provide critical information about the growth mechanism (geometrical and electronic structure) and the origin of fcc-structure formation for the thiolate-protected gold nanoclusters.

Atomically precise ligand-protected gold nanoclusters (<2 nm) have attracted great research interest[1−4] because of their peculiar properties, such as intrinsic chirality,[2,5−11] catalysis,[12−15] biomedicine,[16] magnetism,[17,18] and photoluminescence.[19−23] Recently, advances in synthesis and structure determination of thiolated gold nanoclusters[24−26,33−41,43,44] as well as theoretical research[27−32] have been achieved. The ultrasmall gold nanoclusters demonstrated diverse Au atom packing structures in contrast to Au(I)−SR complexes and larger gold nanoparticles (>2 nm). For example, (*i*) gold nanoclusters can form different crystallographic structures, such as hexagonal closed packed (hcp),[33−35] body-centered cubic (bcc),[36] and face-centered cubic (fcc) structures.[37−41] In contrast, the large gold nanoparticles and bulk gold adopt the fcc-structure. (*ii*) The HOMO−LUMO transition in larger gold nanoclusters involves sp ← sp intraband excitation,[25,42] while small gold nanoclusters (e.g., $Au_{18}(SR)_{14}$) and the Au(I) complexes mainly involve sp ← d interband excitation for the HOMO−LUMO transition.[33,34]

Despite great experimental and theoretical research efforts, some fundamental issues about the geometrical and electronic structure evolution of thiolate-stabilized gold nanclusters remain to be addressed. The first issue is about the origin of fcc kernel formation. Recently, a series of fcc-structured gold nanoclusters has been reported, e.g. $Au_{23}(SR)_{16}^-$, $Au_{28}(TBBT)_{20}$, $Au_{30}S(SR)_{18}$, $Au_{36}(SR)_{24}$, $Au_{40}(SR)_{24}$, $Au_{44}(SR)_{28}$, and $Au_{52}(SR)_{32}$.[37−41] These reported nanoclusters show an interesting tendency, i.e., the growth of the fcc-structure via assembly of cuboctahedral units. However, the formation mechanism of the cuboctahedral unit as well as the edge size of the thiolated gold cluster which forms the first cuboctahedral unit is not clear. Second, the smaller gold nanoclusters (e.g., $Au_{18}(SR)_{14}$) and the Au(I) complexes typically show sp ← d interband excitation in the HOMO−LUMO transition.[33,34] In contrast, the HOMO−LUMO transition of the larger nanoclusters (i.e., 8e or more free valence electrons) mainly involves sp ← sp excitation.[25,42] Is the transition of the electronic excitation mode from sp ← d to sp ← sp caused by the increase of cluster size/Au-kernels or other factors, such as the increased number of free metal electrons? Research on these questions will help to obtain a deeper level of understanding of the geometrical and electronic structure evolution of thiolate-stabilized gold nanoclusters.

Herein, we use HS-Adm (adamantanethiol) as ligand to convert the $Au_{18}(SR)_{14}$ nanocluster into a new nanocluster formulated as $Au_{21}(S\text{-}Adm)_{15}$ with its structure solved by X-ray crystallography (Figure 1). Note that we have tried many ligands such as 4-*tert*-butylbenzenethiolate and *tert*-butyl mercaptan, etc., as shown in Figure S1; however, only HS-Adm can induce the growth of hcp-structured Au_{18} nanoclusters to fcc-structured Au_{21} nanoclusters. Interestingly, the HOMO−LUMO transition in $Au_{21}(S\text{-}Adm)_{15}$ exhibits an sp ← sp intraband transition, in contrast with the sp ← d interband transition in the $Au_{18}(SR)_{14}$, and more importantly, the hcp-structured Au_9 core in $Au_{18}(SR)_{14}$ grows to a fcc-structured Au_{10} core in the $Au_{21}(SR)_{15}$ nanocluster. This new nanocluster is also the first report of a thiolated gold nanocluster which has six free valence electrons. Together with the density functional theory (DFT) calculation, the critical information about the origin of the fcc-structure, the growth mechanism of thiolated gold nanoclusters, and the electronic structure evolution (from sp ← d to sp ← sp) of gold nanoclusters are studied.

The $Au_{21}(SR)_{15}$ nanocluster is composed of two octahedrons sharing one edge (Figure 2a and 2b) instead of sharing one face

Received: June 10, 2016
Published: August 23, 2016

DOI: 10.1021/jacs.6b06004
J. Am. Chem. Soc. 2016, 138, 10754−10757

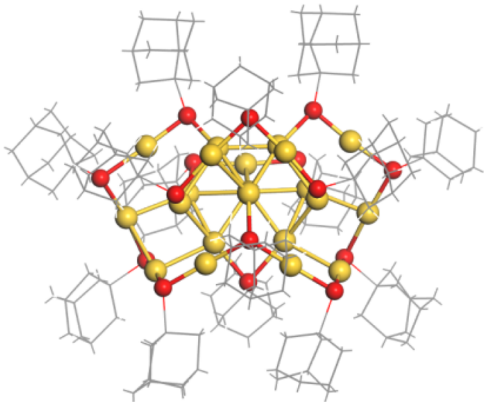

Figure 1. Total structure of the $Au_{21}(S\text{-}Adm)_{15}$ nanocluster. Labels: yellow = Au, red = S, gray = C, white = H. The carbon tails are in wireframe mode.

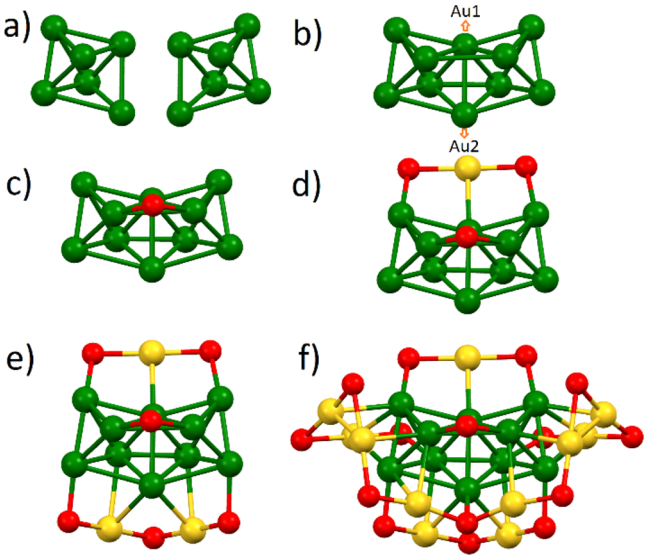

Figure 2. (a,b) Au_{10} kernel structure in the $Au_{21}(S\text{-}Adm)_{15}$ nanocluster. (c–f) Thiolate binding modes in the $Au_{21}(S\text{-}Adm)_{15}$ nanocluster: (c) bridge thiolate; (d) with $Au(SR)_2$ staples; (e) with $Au_2(SR)_3$ unit; (f) further capped by $Au_8(SR)_9$ motifs (green and yellow = Au; red = S).

as in the $Au_{18}(SR)_{14}$ nanocluster. The radial Au–Au bond lengths in Au_{21} give an average of 2.86 Å (close to the distance in bulk gold, 2.88 Å), which is 1.45% shorter than the average distance of the Au_9 kernel in the Au_{18} nanocluster. This kernel is protected by four different motif structures: (*i*) a bridging thiolate that binds two kernel gold atoms (Figure 2c); (*ii*) a $Au(SR)_2$ monomeric staple (Figure 2d); (*iii*) a $Au_2(SR)_3$ dimeric staple (Figure 2e); and (*iv*) a very long $Au_8(SR)_9$ staple motif (Figure 2f). Note that the longest motif before this work was the $Au_8(SR)_8$ ring in the Au_{20} nanocluster.[44] In the Au_{10} core, we found two gold atoms (Figure 2b, labeled by Au1 and Au2, respectively) that have an unusual coordinating structure. From Figure 2f, the Au1 atom is coordinated with the Au(I) atom in a monomeric motif and the Au2 is protected by a –SAdm group in the $[Au_8(SR)_9]$ motif. The distance between the Au2 and S atoms is 2.462 Å, which is longer than the regular bond length of Au(I)–S (~2.3 Å).

DFT calculation was performed to reveal the possible growth mechanism from a Au_{18} to a Au_{21} nanocluster. As shown in Figure 3a, starting from the $Au_{18}(SR)_{14}$ cluster, we considered an exterior Au atom (Figure 3a and 3b, labeled by 3) is inserted

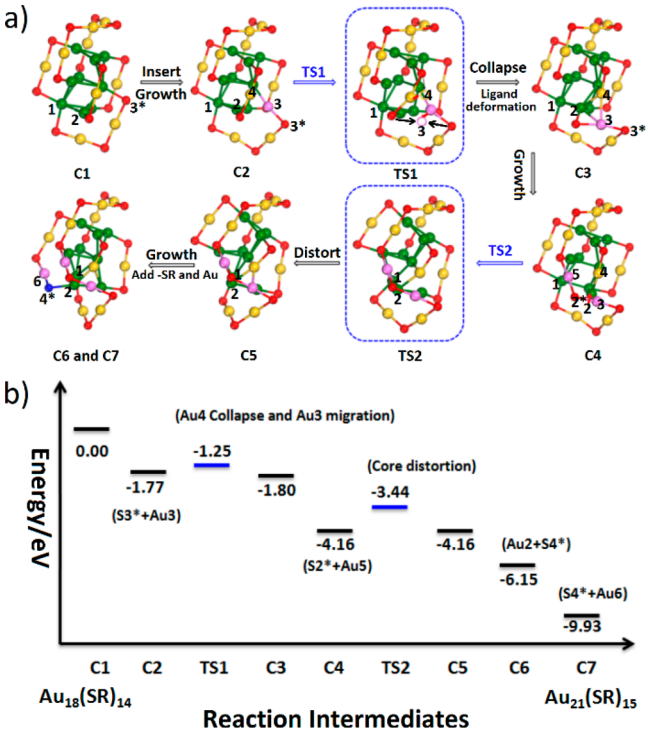

Figure 3. (a) Proposed intermediate structures for the step-by-step conversion of $Au_{18}(SCH_3)_{14}$ to $Au_{21}(SCH_3)_{15}$. (b) Computed reaction energies for each conversion step described in part a. (Pink, yellow, and green = Gold; red = S; atoms labeled with numbers are Au; atoms labeled with numbers and * are S.)

into an Au-SR bond (**C2** in Figure 3a). After that, a structural isomerization is considered, where an Au-SR bond in the monomeric staple motif is broken and a new trimeric motif is formed. As shown in step **C2** → **C4**, this process includes the collapse of a motif Au(I) atom (labeled by **4**) into the Au-core and the migration of a gold atom (labeled by **3**) to the position between two thiolate groups to form a trimeric motif. The transition state for this rearrangement process is determined (**TS1**). The energy barrier is 0.52 eV. After this rearrangement process, the cluster energy is slightly decreased by 0.03 eV. Following the rearrangement step, another exterior Au atom is further introduced, which binds two thiolate groups and forms a longer staple motif containing eight Au(I) atoms (**C4** in Figure 3). An isomerization process is further considered by rotating a triangular Au_3 unit at the bottom of the cluster (step **C4** → **C5**). As shown in Figure 3a and 3b, in this isomerization process, a tetrahedron Au_4 and a new triangular Au_3 unit are formed. The energy barrier for the isomerization step is 0.72 eV. Finally, a thiolate and an exterior Au atom are added to finish the growth of cluster to $Au_{21}(SR)_{15}$. The energy change during this growth path way is given in Figure 3b.

The proposed growth processes suggested a simple growth principle of gold nanoclusters, which includes three key steps: (*i*) Core-growth triggered by an exterior Au atom; that is, an Au atom is first inserted into an Au–S bond. (*ii*) Collapse and growth; that is, the motif gold atom collapsed into the core to finish the core-growth. (*iii*) The exposed thiolate ligand and/or core gold atom in this step provides active sites to the growth of new ligand motifs.

DOI: 10.1021/jacs.6b06004
J. Am. Chem. Soc. 2016, 138, 10754–10757

The significant change of the Au-core structure from hcp to fcc caused by addition of an extra gold atom provides a clue for understanding the cuboctahedral unit formation in the thiolate-stabilized gold clusters. As shown in Figure 4a, in the Au_{18}

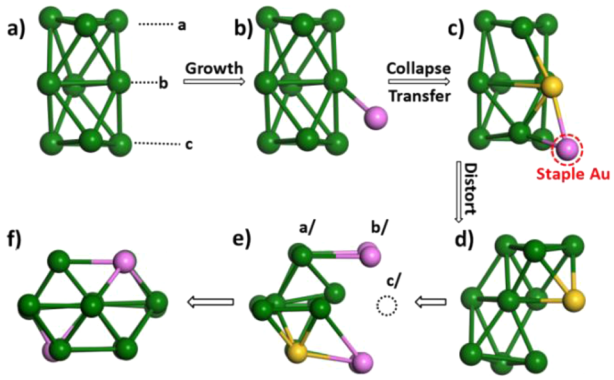

Figure 4. Proposed fcc formation process. (a) Au_9 hcp core in a $Au_{18}(SR)_{14}$ nanocluster; (b) adding one gold to the Au-core; (c) collapse of the gold(I) atom; (d) structure distortion; (e) with four gold atoms in the motif structure; (f) complete cuboctahedron unit in the $Au_{23}(SR)_{16}^-$ nanocluster. (green = Au in the kernel; pink = additional Au; yellow = Au in the motif structure).

nanocluster, two octahedrons share one triangular face. When the additional Au atom is added to the kernel (Figure 4b), a motif gold(I) atom will collapse into the core and the previously added Au atom migrates into the ligand shell. These two steps do not change the arrangement of gold atoms in the metal core. After that, this center and the bottom trigonal Au_3 undergo distortions (Figure 4d). This Au_{10} core, together with four motif gold atoms (Figure 4e, labeled in pink color), become an fcc-structured cuboctahedron (note, one gold atom is missing). The {111} planes are indexed as a, b, and c. With the growth of the nanocluster, the complete fcc cuboctahedron unit could be found in the Au_{23} nanocluster by filling up the missing gold and further growth to larger fcc-structured gold nanoclusters, such as $Au_{28}(SR)_{20}$,[38] $Au_{30}S(SR)_{18}$,[40,41] $Au_{36}(SR)_{24}$,[38] and $Au_{333}(SR)_{79}$,[46] and finally to large gold nanoparticles.

Previous work revealed that thiolated gold nanoclusters of no more than 4e (e.g., 2e $Au_{15}(SR)_{13}$, 4e $Au_{18}(SR)_{14}$, $Au_{20}(SR)_{16}$, and $Au_{22}(SR)_{18}$) are dominated by sp ← d excitations.[29,33,34,44,45] (Figure 5, Figure S2 and Table S1). Meanwhile, the HOMO−LUMO peak of gold nanoclusters with 8e or more (e.g., 8e $Au_{23}(SR)_{16}^-$, $Au_{25}(SR)_{18}^-$, and 12e $Au_{36}(SR)_{24}$ etc.) is dominated by sp ← d excitations. The $Au_{21}(SR)_{15}$ nanocluster in the current work has 6e, which bridges up the previous 4e and 8e gold nanoclusters. As shown in Figure 5, the HOMO−LUMO transition is due to the Au sp ← sp excitation. In view of the excitation mode change from the 4e to 6e gold clusters, we suggest that the emergence of sp ← sp excitation in the thiolate-stabilized gold clusters is most likely caused by the increase of the cluster free valence electron. The 6e $Au_{21}(SR)_{15}$ cluster is at this transition edge.

Finally, the adaptive natural density partitioning (AdNDP) analysis[47] is carried out to figure out the interesting question about the 2e increase during the cluster growth. Considering each ligand motif can bind one free metal valence electron of the Au-core, the Au_9-core in $Au_{18}(SR)_{14}$ and the Au_{10}-core in $Au_{21}(SR)_{15}$ can be considered as Au_9^{5+} or Au_{10}^{4+} species, respectively. From Figure 6, it is seen that during the

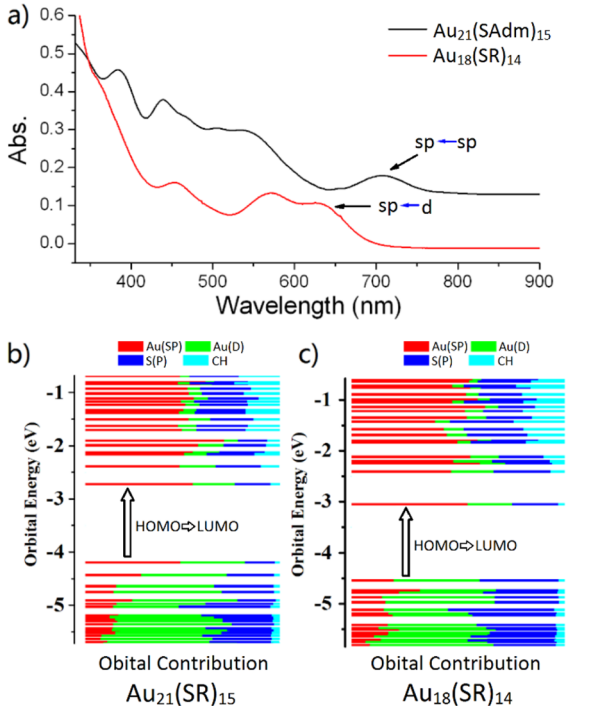

Figure 5. (a) UV/vis spectra of $Au_{21}(SR)_{15}$ and $Au_{18}(SR)_{14}$ nanoclusters. (b and c) Kohn−Sham orbitals of $Au_{21}(SCH_3)_{15}$ and $Au_{18}(SCH_3)_{14}$ nanoclusters, respectively. The orbital is drawn to indicate the relative contributions (line length with color labels) of the atomic orbitals of Au(6sp) (red), Au(5d) (green), and S(3p) (blue), and other orbital contributions from C and H atoms (cyan).

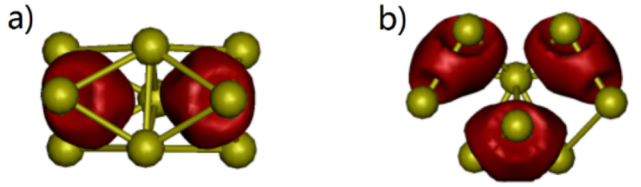

Figure 6. (a) Visualization of the 4e valence electron distribution in the Au_9^{5+}. (b) Visualization of the 6e valence electron distribution in the Au_{10}^{4+}. The AdNDP analysis is applied for free valence electron distribution analysis.

transformation of the Au-core from the face-sharing bioctahedron (in $Au_{18}(SR)_{14}$) to the edge-sharing bioctahedron Au-core (in $Au_{21}(SR)_{16}$), the valence electrons distribution corresponds to a transition from localization in two Au_6-octahedrons to distribution in a tetrahedron Au_4 unit and two Au_3-units, respectively. It is known that the Au_4-tetrahedron is the basic unit in the fcc-structure. Upon changing the Au-core from hcp to fcc configuration, 2e are localized on the Au_4-unit. The remaining 4e are distributed evenly on two symmetric Au_3-units, respectively. The evolution of the superatom-like electronic structures from the Au_{18} to Au_{21} nanoclusters is investigated as well. As displayed in Figure S3, the superatomic electronic configurations of $1S^2|1P^2$ and $1S^2|1P^4$ are found in the Au_9^{5+} or Au_{10}^{4+} species. The partially 1P shell corresponds to the nonspherical shape of the clusters.

In conclusion, a new nanocluster formulated as Au_{21}(S-Adm)$_{15}$ is obtained via a strategy of ligand-induced conversion of Au_{18} to Au_{21}, and the total structure is determined. The determined atomic structure of Au_{21}(S-Adm)$_{15}$ shows transformation of the Au-kernel from hcp to fcc-structure, which

DOI: 10.1021/jacs.6b06004
J. Am. Chem. Soc. 2016, 138, 10754−10757

provides an intermediate for further growth of the cuboctahedral unit. DFT simulations of the conversion reveal a collapse of the surrounding gold atoms and then structural distortion. Accompanied by the Au-core transformation, the HOMO−LUMO transition undergoes a transition from sp ← d interband excitation to sp ← sp intraband transition. The nature of the cluster free valence electron increase from 4e to 6e is correlated with the Au-core growth from face-sharing bioctahedron Au_9 to edge-sharing Au_{10}, where the free valence electrons take different distribution manners in the Au-cores. Our work will benefit fundamental understanding of the geometrical structure and electronic structure of gold nanomaterial at the atomic level.

■ ASSOCIATED CONTENT

Supporting Information

The Supporting Information is available free of charge on the ACS Publications website at DOI: 10.1021/jacs.6b06004.

Details of the synthesis and X-ray crystallographic analysis (PDF)

CIF of $Au_{21}(S\text{-}Adm)_{15}$(CIF)

■ AUTHOR INFORMATION

Corresponding Authors

*ixing@ahu.edu.cn

*ypnku78@gmail.com

*zmz@ahu.edu.cn

Author Contributions

‖S.C. and L.X. contributed equally.

Notes

The authors declare no competing financial interest.

■ ACKNOWLEDGMENTS

We acknowledge financial support by NSFC (21372006, U1532141, 21373176, 21422305), the Ministry of Education and Ministry of Human Resources and Social Security, the Education Department of Anhui Province, Anhui Province International Scientific and Technological Cooperation Project, 211 Project of Anhui University, Hunan Provincial Natural Science Foundation of China (12JJ1003), and Scientific Research Fund of Hunan Provincial Education Department (13A100).

■ REFERENCES

(1) Qian, H.; Zhu, M.; Wu, Z.; Jin, R. *Acc. Chem. Res.* **2012**, *45*, 1470.

(2) Knoppe, S.; Burgi, T. *Acc. Chem. Res.* **2014**, *47*, 1318.

(3) Maity, P.; Xie, S.; Yamauchi, M.; Tsukuda, T. *Nanoscale* **2012**, *4*, 4027.

(4) Jin, R. *Nanoscale* **2015**, *7*, 1549.

(5) Dolamic, I.; Knoppe, S.; Dass, A.; Burgi, T. *Nat. Commun.* **2012**, *3*, 798.

(6) Dolamic, I.; Varnholt, B.; Burgi, T. *Nat. Commun.* **2015**, *6*, 7117.

(7) Barrabes, N.; Zhang, B.; Burgi, T. *J. Am. Chem. Soc.* **2014**, *136*, 14361.

(8) Wan, X. K.; Yuan, S. F.; Lin, Z. W.; Wang, Q. M. *Angew. Chem., Int. Ed.* **2014**, *53*, 2923.

(9) Zhu, M.; Qian, H.; Meng, X.; Jin, S.; Wu, Z.; Jin, R. *Nano Lett.* **2011**, *11*, 3963.

(10) Xiao, D.; Yang, W.; Yao, J.; Xi, L.; Yang, X.; Shuai, Z. *J. Am. Chem. Soc.* **2004**, *126*, 15439.

(11) Ke, D.; Tang, A.; Zhan, C.; Yao, J. *Chem. Commun.* **2013**, *49*, 4914.

(12) Wang, S.; Jin, S.; Yang, S.; Chen, S.; Song, Y.; Zhang, J.; Zhu, M. *Sci. Adv.* **2015**, *1*, e1500441.

(13) Chong, H.; Li, P.; Wang, S.; Fu, F.; Xiang, J.; Zhu, M.; Li, Y. *Sci. Rep.* **2013**, *3*, 3214.

(14) Erickson, J. D.; Mednikov, E. G.; Ivanov, S. A.; Dahl, L. F. *J. Am. Chem. Soc.* **2016**, *138*, 1502.

(15) Li, G.; Jin, R. *J. Am. Chem. Soc.* **2014**, *136*, 11347.

(16) Rosi, N. L.; Giljohann, D. A.; Thaxton, C. S.; Lytton-Jean, A. K. R.; Han, M. S.; Mirkin, C. A. *Science* **2006**, *312*, 1027.

(17) Zhu, M.; Aikens, C. M.; Hendrich, M. P.; Gupta, R.; Qian, H.; Schatz, G. C.; Jin, R. *J. Am. Chem. Soc.* **2009**, *131*, 2490.

(18) Antonello, S.; Perera, N. V.; Ruzzi, M.; Gascon, J. A.; Maran, F. *J. Am. Chem. Soc.* **2013**, *135*, 15585.

(19) Ghosh, A.; Udayabhaskararao, T.; Pradeep, T. *J. Phys. Chem. Lett.* **2012**, *3*, 1997.

(20) Li, G.; Lei, Z.; Wang, Q. M. *J. Am. Chem. Soc.* **2010**, *132*, 17678.

(21) Kang, X.; Wang, S.; Song, Y.; Jin, S.; Sun, G.; Yu, H.; Zhu, M. *Angew. Chem., Int. Ed.* **2016**, *55*, 3611.

(22) Wang, S.; Meng, X.; Das, A.; Li, T.; Song, Y.; Cao, T.; Zhu, X.; Zhu, M.; Jin, R. *Angew. Chem., Int. Ed.* **2014**, *53*, 2376.

(23) Yao, Q.; Yuan, X.; Yu, Y.; Yu, Y.; Xie, J.; Lee, J. Y. *J. Am. Chem. Soc.* **2015**, *137*, 2128.

(24) Jadzinsky, P. D.; Calero, G.; Ackerson, C. J.; Bushnell, D. A.; Kornberg, R. D. *Science* **2007**, *318*, 430.

(25) Zhu, M.; Aikens, C. M.; Hollander, F. J.; Schatz, G. C.; Jin, R. *J. Am. Chem. Soc.* **2008**, *130*, 5883.

(26) Heaven, M. W.; Dass, A.; White, P. S.; Holt, K. M.; Murray, R. W. *J. Am. Chem. Soc.* **2008**, *130*, 3754.

(27) Pei, Y.; Gao, Y.; Shao, N.; Zeng, X. C. *J. Am. Chem. Soc.* **2009**, *131*, 13619.

(28) Pei, Y.; Pal, R.; Liu, C.; Gao, Y.; Zhang, Z.; Zeng, X. C. *J. Am. Chem. Soc.* **2012**, *134*, 3015.

(29) Jiang, D. E.; Overbury, S. H.; Dai, S. *J. Am. Chem. Soc.* **2013**, *135*, 8786.

(30) Lopez-Acevedo, O.; Akola, J.; Whetten, R. L.; Grönbeck, H.; Häkkinen, H. *J. Phys. Chem. C* **2009**, *113*, 5035.

(31) Pei, Y.; Zeng, X. C. *Nanoscale* **2012**, *4*, 4054.

(32) Shichibu, Y.; Zhang, M.; Kamei, Y.; Konishi, K. *J. Am. Chem. Soc.* **2014**, *136*, 12892.

(33) Chen, S.; Wang, S.; Zhong, J.; Song, Y.; Zhang, J.; Sheng, H.; Pei, Y.; Zhu, M. *Angew. Chem., Int. Ed.* **2015**, *54*, 3145.

(34) Das, A.; Liu, C.; Byun, H. Y.; Nobusada, K.; Zhao, S.; Rosi, N.; Jin, R. *Angew. Chem., Int. Ed.* **2015**, *54*, 3140.

(35) Higaki, T.; Liu, C.; Zeng, C.; Jin, R.; Chen, Y.; Rosi, N. L.; Jin, R. *Angew. Chem., Int. Ed.* **2016**, *55*, 6694.

(36) Liu, C.; Li, T.; Li, G.; Nobusada, K.; Zeng, C.; Pang, G.; Rosi, N.; Jin, R. *Angew. Chem., Int. Ed.* **2015**, *54*, 9826.

(37) Das, A.; Li, T.; Nobusada, K.; Zeng, C.; Rosi, N.; Jin, R. *J. Am. Chem. Soc.* **2013**, *135*, 18264.

(38) Zeng, C.; Chen, Y.; Iida, K.; Nobusada, K.; Kirschbaum, K.; Lambright, K. J.; Jin, R. *J. Am. Chem. Soc.* **2016**, *138*, 3950.

(39) Zeng, C.; Chen, Y.; Liu, C.; Nobusada, K.; Rosi, N. L.; Jin, R. *Sci. Adv.* **2015**, *1*, e1500425.

(40) Yang, H.; Wang, Y.; Edwards, A. J.; Yan, J.; Zheng, N. *Chem. Commun.* **2014**, *50*, 14325.

(41) Crasto, D.; Malola, S.; Brosofsky, G.; Dass, A.; Häkkinen, H. *J. Am. Chem. Soc.* **2014**, *136*, 5000.

(42) Pei, Y.; Gao, Y.; Zeng, X. C. *J. Am. Chem. Soc.* **2008**, *130*, 7830.

(43) Das, A.; Li, T.; Li, G.; Nobusada, K.; Zeng, C.; Rosi, N. L.; Jin, R. *Nanoscale* **2014**, *6*, 6458.

(44) Zeng, C.; Liu, C.; Chen, Y.; Rosi, N. L.; Jin, R. *J. Am. Chem. Soc.* **2014**, *136*, 11922.

(45) Pei, Y.; Tang, J.; Tang, X.; Huang, Y.; Zeng, X. C. *J. Phys. Chem. Lett.* **2015**, *6*, 1390.

(46) Qian, H.; Zhu, Y.; Jin, R. *Proc. Natl. Acad. Sci. U. S. A.* **2012**, *109*, 696.

(47) (a) Zubarev, D. Y.; Boldyrev, A. I. *Phys. Chem. Chem. Phys.* **2008**, *10*, 5207−5217. (b) Zubarev, D. Y.; Boldyrev, A. I. *J. Phys. Chem. A* **2009**, *113*, 866−868.

DOI: 10.1021/jacs.6b06004
J. Am. Chem. Soc. 2016, 138, 10754−10757